



# Thermal error prediction of ball screws in full-time series using working condition data based on a mechanism and data hybrid-driven model

Min Wang<sup>1</sup> · Wenlong Lu<sup>1</sup> · Kuan Zhang<sup>1</sup> · Xiaofeng Zhu<sup>2</sup> · Mengqi Wang<sup>2</sup> · Bo Yang<sup>2</sup> · Xiangsheng Gao<sup>1</sup>

Received: 3 October 2023 / Accepted: 13 May 2024 / Published online: 1 June 2024

© The Author(s), under exclusive licence to Springer-Verlag London Ltd., part of Springer Nature 2024

## Abstract

The ball screw is a vital component in the feed drive systems of machine tools. It is susceptible to thermal errors that significantly impact its accuracy. Current thermal error modeling methods for ball screws face significant challenges in achieving full-time series prediction. Furthermore, these methods impose stringent requirements for a complex temperature data collection process, further constrained by the compact structure of machine tools. Additionally, valuable working condition data in thermal error prediction remains underutilized. This paper proposes a new hybrid-driven model that combines mechanism and data-driven approaches to achieve full-time series thermal error prediction of ball screws. The proposed model utilizes the operating rotational speed as a key input parameter, eliminating the need for temperature collection during the modeling stage and the compensation process. The temperature model is proposed as a mechanism-driven model based on heat transfer theory to calculate the temperature of the thermal sensitive points by utilizing operating rotational speed. The accuracy of the model is validated through thermal characteristic experiments of ball screws under four different working conditions. The data-driven models based on different traditional neural networks are established to predict thermal errors according to the time series temperature data from the temperature model. Moreover, hyperparameters of different neural networks are optimized by the Beetle Antennae Search (BAS). Comparative analysis among different neural network-based hybrid-driven models reveals that the convolutional neural network (CNN) model optimized by BAS consistently exhibits lower absolute errors predominantly below 10  $\mu\text{m}$ , as well as lower root mean squared error (RMSE) and mean absolute error (MAE) values in each working condition. The BAS-CNN model, within the hybrid-driven model framework, is better suited for the full-time series prediction of thermal errors in ball screws. The BAS-CNN model is a foundation for thermal error compensation by utilizing working condition data.

**Keywords** Ball screws · Thermal error prediction · Hybrid-driven model · Neural network

## 1 Introduction

Thermally induced errors contribute substantially to the overall error affecting the machining accuracy [1], particularly given the current high-speed trend in machine tools. The thermal-induced errors account for as much as

75% of the machined geometric errors [2]. Thermal errors can generally be attributed to the thermal deformations of the machine elements caused by heat sources within the structure, i.e., ball screws, bearings, nuts, axis drive motors, friction on the surfaces, cutting processes, the flow of coolant/lubricating oil, and the ambient temperature [3]. The ball screw feed drive system (BSFDS) is a crucial and indispensable transmission mechanism responsible for converting the motor-generated rotational motion into the linear motion of a nut-driven carriage. However, the thermal elastic deformation of ball screws resulting from heat generation in the motor, nuts, and bearings causes thermal errors that significantly impact machining accuracy. Hence, it is imperative to undertake research aimed at

✉ Xiangsheng Gao  
gaosh@bjut.edu.cn

<sup>1</sup> Beijing Key Laboratory of Advanced Manufacturing Technology, Faculty of Materials and Manufacturing, Beijing University of Technology, Beijing 100124, China

<sup>2</sup> Beijing Precision Machinery & Engineering Research Co., LTD, No.22 Tianzhu West Road, Shunyi District, Beijing 101300, China

mitigating the thermal effects of the ball screw, enhancing the position accuracy of machine tools.

Thermal error avoidance/control and thermal error modeling/compensation are the two solutions for reducing thermal errors of BSFDS. Engineers tend to design and optimize the structure of the machine [4], add a cooling system [5, 6], separate the heat source, control the room temperature of the workshop, use new materials with high thermal conductivity [7] or the negative coefficient of thermal expansion [8], or employ real-time active thermal control method [2]. However, certain approaches necessitate modifying the machine tool structure or incorporating new systems, requiring a profound comprehension of the machine tool's structure. Additionally, certain methods introduce new materials, increasing the concerns regarding material durability.

Thermal error compensation is a cost-effective strategy to offset thermal-induced errors by actively introducing controlled errors into the system, improving machining accuracy without necessitating modifications to the machine tool's structure. The effectiveness of compensation relies heavily on precise temperature measurements at sensitive points and accurate prediction of thermal errors during machining operations. Consequently, establishing a thermal error model with high prediction accuracy and robustness is the fundamental basis for thermal error compensation. Nevertheless, given the nonlinear nature of thermal errors and the constantly ever-changing and intricate working conditions, accurately capturing the variation pattern of thermal errors using a model remains challenging.

Theoretical and empirical modeling are the two main modeling methods for thermal errors. Theoretical modeling involves utilizing heat transfer theory and appropriate boundary conditions to solve the temperature distribution and thermal error. In more intricate scenarios, these parameters are commonly obtained via finite element analysis (FEA) [9, 10]. The finite element modeling method's precision hinges on the boundary conditions' accuracy. However, obtaining accurate heat source intensity and boundary conditions is challenging due to the nonlinear temperature increase in BSFDS. Additionally, applying the FEA method is constrained by its time-consuming nature, limiting its widespread usage [11]. Empirical modeling directly builds a mapping relationship between the machine tool working conditions and the volumetric thermal error based on experimental data [2].

The general steps of empirical modeling include selecting thermal key points and using algorithms to establish a mapping relationship between thermal key points' temperature and thermal errors. The temperature field of BSFDS can be mainly reflected by the temperature of thermal sensitive points [11]. Frequently used algorithms for thermal error modeling include the least square method, multiple

regression analyses, grey system, support vector machine (SVM), hybrid model, and neural networks [12].

Jiang and Yang [13] successfully fitted the thermal drift error curve of the spindle by employing the Chebyshev polynomial-based orthogonal least squares regression method. The authors concluded that the resulting curve agreed with the measurement error curve. Specifically, the maximum modeling residuals in the X, Y, and Z directions were found within the ranges of 0.8–1  $\mu\text{m}$ , 0.6–0.9  $\mu\text{m}$ , and 1.2–1  $\mu\text{m}$ , respectively. Pajor and Zapłata [14] developed an analytical model for the spindle using the multiple regression approach. The authors reduced the thermal error from 73 to 13  $\mu\text{m}$  by applying this model for thermal error compensation of the spindle. Despite these two methods' relatively simple model structure and reliable performance, their predictive ability in complex conditions is low. Jiang and Yang [15] employed a genetic algorithm to optimize the dimensions and variable weights of a new gray system model based on the standard gray system model GM (1, 1) to minimize the residual value of the optimized model. The resultant optimized model captures the systematic trend of thermal errors and mitigates the impact of random fluctuations in thermal error, improving the prediction accuracy of the thermal error model. Although it does not depend on extensive and comprehensive data information, the model will be different when the input is altered, and its convergence speed is relatively slow.

Zhang et al. [16] incorporated the grid search method to optimize the penalty and kernel of the SVM thermal error model, enhancing the model's performance. Significant reductions of 89.55% and 85.67% were achieved in the X-axis positioning error and Z-axis positioning error by applying the optimized model to the X and Z axes of the CNC platform, respectively. SVM demonstrates strong nonlinear function fitting capability [17]. However, it necessitates significant computing resources, exhibits slow convergence speed, and presents challenges in parameter selection.

Neural network, an emerging data-driven modeling method originating from artificial intelligence, has found widespread application in thermal error prediction. The thermal errors of machine tools in multiple directions can be accurately fitted and predicted after the network's learning and training [18, 19]. Since single modeling methods often struggle to perform well, hybrid modeling methods have been proposed to compensate for their shortcomings. GA, particle swarm optimization (PSO), and grey theory have been adopted into the neural network to optimize the initial value and increase the accuracy, convergence, and robustness [11]. However, mechanism and data hybrid-driven models in thermal error compensation have not been reported.

Ma et al. [20] optimized BP algorithm with GA and PSO, enhancing the machining accuracy of a borer spindle system

in a precision jig by 67% and 89%, respectively. Tan [21] combined multiple BP neural network models to enhance predictive performance. The integrated model was applied to a horizontal machining center THM6380, resulting in an RMSE of 5.6522  $\mu\text{m}$ , demonstrating improved accuracy in prediction. BP neural networks have high robustness and fault tolerance ability. However, their convergence speed is slow and can easily fall into value-extremum. Zhang et al. [22] improved the radial basis function (RBF) neural network and developed a thermal error prediction model by utilizing the PSO algorithm to optimize critical parameters of the RBF neural network. Zhang et al. [23] employed fuzzy clustering and grey relational analysis techniques to optimize the placement of temperature measurement points. Subsequently, the authors developed a radial basis function neural network prediction model using a genetic algorithm. The enhanced model exhibits enhanced accuracy and increased robustness compared to the conventional RBF neural network approach. Moreover, the residual error of the forecasting model was reduced from 4.88 to 3.80  $\mu\text{m}$  to 2.48–2.14  $\mu\text{m}$ . However, extracting key feature functions poses a challenging task in utilizing RBF neural networks. Gao et al. [24] introduced a thermal error prediction method based on PSO and long short-term memory (LSTM) neural networks. Comparative analysis of the performance of PSO-LSTM, BP, and RBF models under various working conditions revealed that the PSO-LSTM model exhibits superior performance and robustness. As data-driven models, neural networks generally exhibit high prediction accuracy and faster training speed.

However, the abovementioned data-driven models encounter difficulties regarding full-time series prediction. This limitation arises because model validation is typically performed solely on a test set representing only a small portion of the entire dataset. Furthermore, all the compensation mentioned above methods necessitate temperature collection processes encompassing the selection of thermal error points, installation of temperature sensors, and precise temperature measurements, serving both thermal error modeling and compensation stages. Unfortunately, these complex temperature collection processes increase installation and maintenance expenses. Moreover, the disregard for the installation location of temperature sensors during the machine tool design phase poses challenges in the subsequent installation of sufficient temperature sensors.

This paper proposes a mechanism and data hybrid-driven model to address the abovementioned problems. Initially, a temperature model based on the heat transfer theory and thermal characteristic parameters of ball screws is proposed and experimentally validated. Furthermore, the data-driven models based on different traditional neural networks are established to predict the thermal error of ball screws with the calculated temperature as input data. Then, BAS is

employed to optimize the hyperparameters of neural networks and improve the model's performance. Finally, the predicted performance of the proposed hybrid-driven model is compared against traditional neural networks.

The hybrid-driven model proposed in this study utilizes working condition data to enable accurate prediction of thermal errors of ball screws in full-time series without temperature data collection. Furthermore, the thermal deformation can be easily converted into thermal error by establishing the relationship between thermal deformation and error during compensation. This study's research logic and roadmap are visually depicted in Fig. 1.

The remainder of this paper is organized as follows. In Section 2, the mechanism and data hybrid-driven modeling method is introduced. The thermal characteristic experiment is conducted to validate the temperature model and provide a dataset for data-driven modeling. In Section 3, the performance of the proposed mechanism and data hybrid-driven models is discussed and compared. The paper is summarized, and the main conclusions are drawn in Section 4.

## 2 Thermal error prediction of ball screws based on a hybrid-driven model

A hybrid-driven model comprising a mechanism-driven model and a data-driven model is proposed for the full-time series prediction of thermally induced errors in ball screws. Firstly, a temperature model of key thermal sensitive points is developed based on heat transfer theory and validated through thermal characteristic experiments. Secondly, data-driven models are proposed based on various traditional neural networks to predict thermal errors. Then, the essential hyperparameters of these deep learning models are optimized using the BAS algorithm. The input and output of the hybrid-driven model are the rotational speed and the thermal deformation of the ball screw, respectively. Finally, the established hybrid-driven model utilizes working condition data of thermal sensitive points instead of measured temperatures to predict thermal errors of ball screws in full-time series.

### 2.1 Mechanism and data hybrid-driven model for thermal error prediction of ball screws

Neural network models based on the time-varying characteristics of the thermal error in the ball screw are employed for regression prediction of the thermal error. A mechanism and data hybrid-driven model is proposed for thermal error prediction by integrating a temperature model, providing calculated temperature data as input for the data-driven model. This part establishes the mapping relationship between working conditions and thermal error. This approach eliminates the need

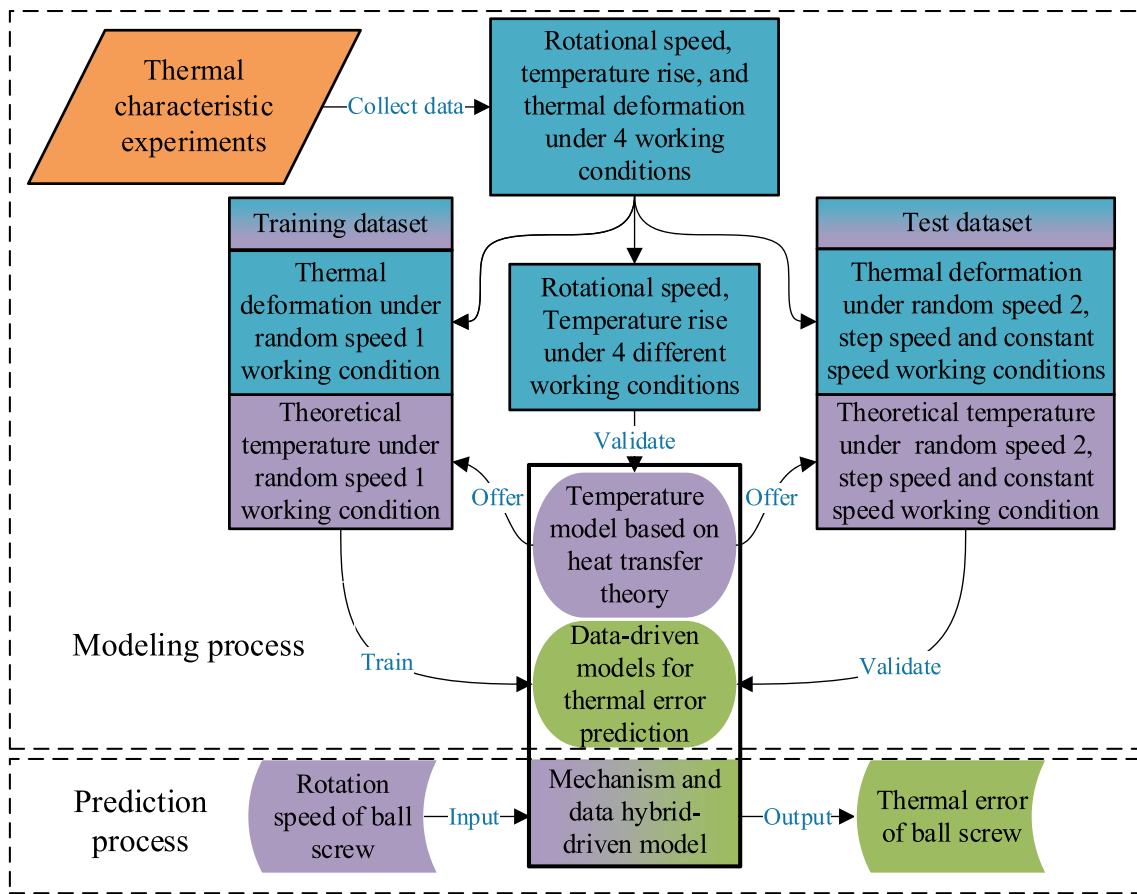
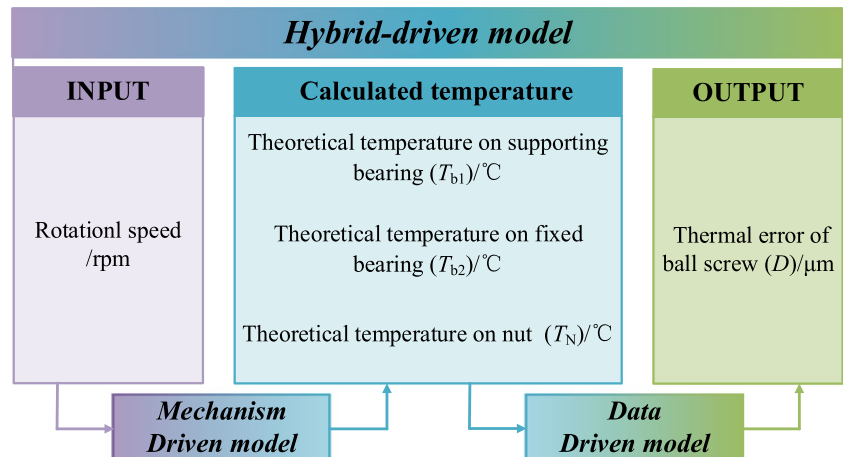


Fig. 1 Research logic and roadmap of this study

for temperature measurements at thermal sensitive points because the temperature is theoretically calculated using the temperature model based on the rotational speed during operation and other related thermal parameters of the ball screw. Consequently, the proposed approach circumvents the complex and costly process of temperature data collection during the

modeling and compensation phases. The mapping relationship between the input and output data of the hybrid-driven model is depicted in Fig. 2. The proposed mechanism and data hybrid-driven model capture the temperature rise mechanism and adjust input parameters to accommodate various working conditions while also possessing the nonlinear mapping

Fig. 2 Mapping relations between input and output data of a hybrid-driven model



capability and self-adaptive characteristics offered by the data-driven model. The mechanism-driven model for theoretical temperature and data-driven model for thermal errors are introduced in order.

## 2.2 Temperature model of ball screws based on heat transfer theory

### 2.2.1 Temperature modeling

A temperature model is developed based on the principles of heat transfer theory and the essential thermal parameters of a specific ball screw test bench to determine the temperature of the key thermal sensitive points on the ball screw. This paper focuses on the high-speed precision ball screw experimental platform as the primary subject of investigation. The primary parameters of the ball screw are presented in Table 1.

In the previous research, three thermal error-sensitive points specifically situated at the contact regions of the fixed bearing, supporting bearing, and nut of the ball screw [24] were identified through thermal modal analysis (TMA). Thus, these three key thermal sensitive points are chosen as the feature points in this study for computing the thermal parameters (Fig. 3).

The variation in temperature of the ball screw primarily arises from the generation of frictional heat at the contact surfaces and the convective heat transfer with the surrounding environment. Therefore, the thermal analysis considers heat generation and diffusion [25]. The real-time temperature of each component of the ball screw was determined based on the operational rotational speed, the thermal boundary conditions of the system, and the relationship between temperature rise and heat transfer by employing the principles of heat transfer theory and utilizing the derived solution for the essential thermal parameters of the ball screw. The temperature rise of each component in the ball screw can be mathematically expressed as follows:

$$T_2 = T_1 + \frac{Q_z}{CM} \tag{1}$$

where  $T_1$  and  $T_2$  represent the initial temperature and the temperature at the specific calculation time of the thermal

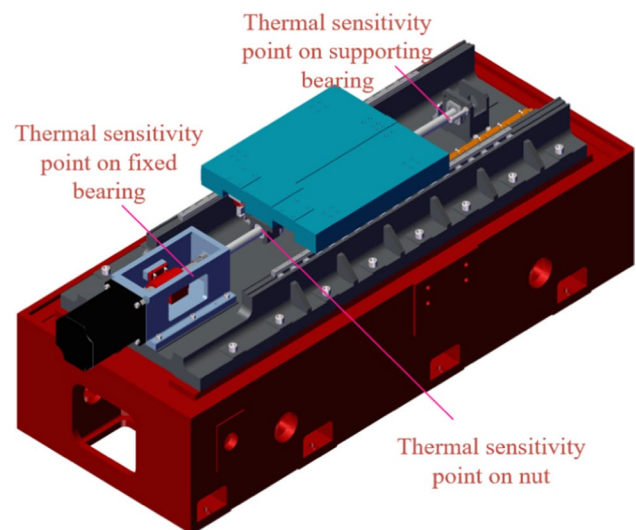


Fig. 3 Thermal sensitive points on the test bench of the ball screw

sensitive point of the ball screw, respectively,  $Q_z$  denotes the total heat absorbed by each component of the ball screw where thermal sensitive points are located,  $C$  signifies specific heat capacity of each component of the ball screw, and  $M$  represents the mass of each component of the ball screw.

The specific solution procedure of the temperature model for calculating the temperature rise of the component at the location of the thermal sensitive point is given in the Appendix.

### 2.2.2 Experimental validation

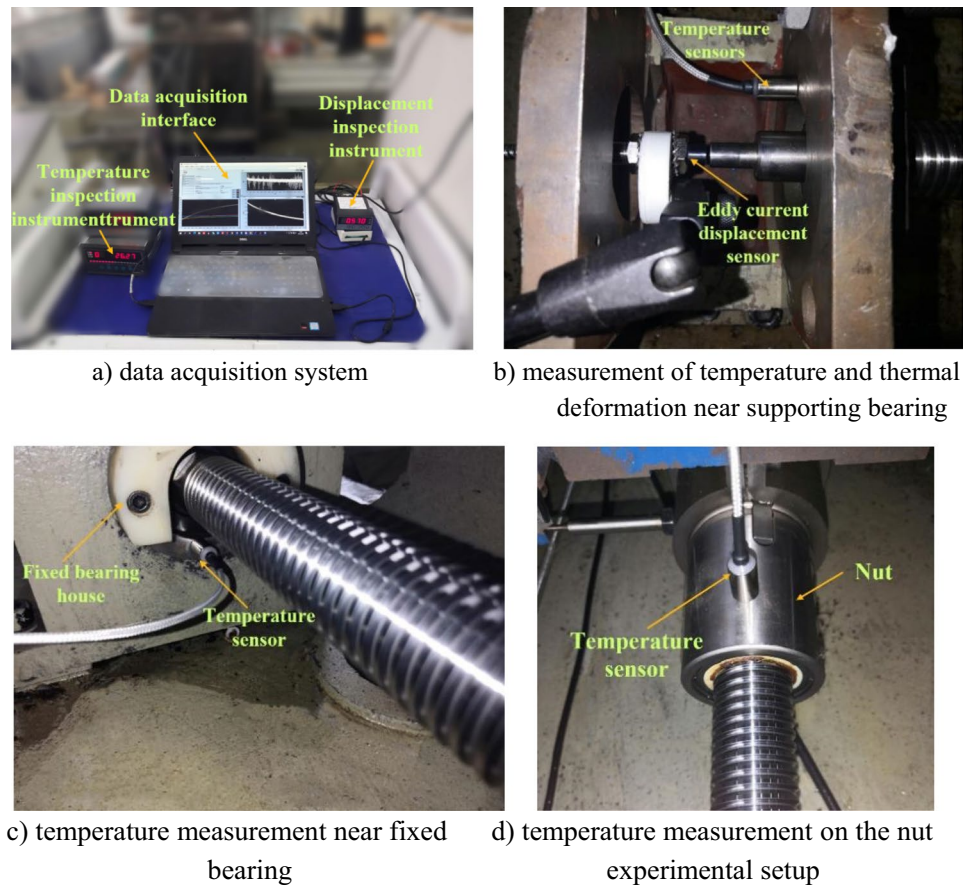
Thermal characteristic experiments were conducted on a high-speed test bench for the precision ball screw under four different working conditions to validate the effectiveness and accuracy of the abovementioned temperature model. The experimental setup and the data acquisition system employed for the experiments are illustrated in Fig. 4. The parameters of the measuring instrument are provided in Table 2. Three temperature sensors were positioned at the fixed bearing, supporting bearing, and nut locations to capture the real-time temperature variation. Additionally, an eddy current displacement sensor was installed at the end face of the screw to measure the thermal deformation.

Four thermal characteristic experiments, comprising two randomly selected speeds, a step speed and a constant speed, were carried out under the rotational speeds specified in Table 3. During the experiments, the nut moves with the screw in the reciprocating cycle. The real-time temperature of the thermal sensitive points and the thermal deformation of the screw were collected during the experiment by a custom-made data acquisition system with a sampling period set at 1 s. After each experiment, a natural cooling period

Table 1 Parameters of the ball screw

Name of parameters	Value
Nominal diameter $d_o$ (mm)	32
Ball diameter $D_b$ (mm)	5.953
Lead $P_h$ (mm)	5
Helix angle $\alpha$ (°)	5.6833
Dynamic load rating $C_a$ (N)	25,628
Length (m)	1.22



**Fig. 4** The experimental setup**Table 2** Parameters of the experimental instrument

Type	Product description
Temperature sensors	KYW-TC, Kunlunyuanyang, Beijing, China
Eddy current displacement sensor	ML33-01-00-03, Milang, Shenzhen, China
Temperature inspection instrument	Kunlunyuanyang, Beijing, China
Displacement inspection instrument	XSAE-CHVB1M2V0, Milang, Shenzhen, China

**Table 3** Rotational speed of four thermal characteristic experiments

Time (min)	0–10	10–20	20–30	30–40	40–50
Random speed 1 (rpm)	400	700	900	500	1000
Random speed 2 (rpm)	300	1000	600	800	700
Step speed (rpm)	500	800	1000	800	500
Constant speed (rpm)	800	800	800	800	800

of 24 h was implemented to allow the temperature of the components to return to ambient temperature conditions.

The temperature of each thermal sensitive point under four working conditions was calculated based on the temperature model according to the rotational speed of the ball screw. Comparative analysis was conducted between the temperature data collected from the thermal characteristic

experiment of the ball screw and the calculated temperature data obtained from the temperature model under four working conditions. The comparative results under random speed 1 are presented in Fig. 5, illustrating a favorable correspondence between the temperature variations of each component and the rotational speed variation of the ball screw. Similar consistency was also observed in the comparative results under the other working conditions (Appendix).

According to the obtained results, it is observed that the calculated temperature data for the supporting bearing exhibits minimal deviation and high accuracy. The calculated temperature data fluctuates around the corresponding experimental temperature data. This indicates a strong agreement between the calculated results of the temperature model and the experimental results in terms of capturing the temperature changes of the supporting bearing.

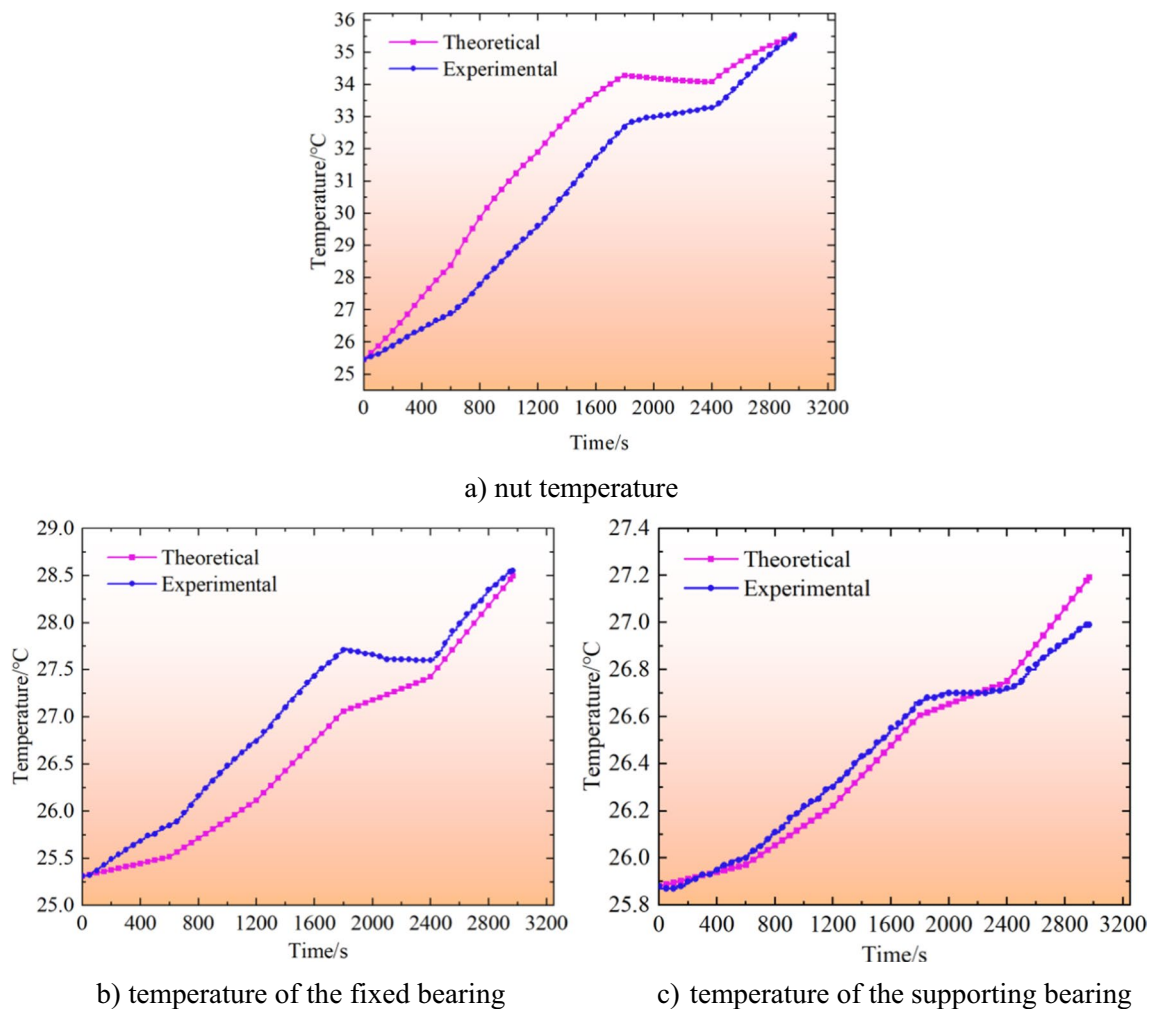


Fig. 5 Temperature comparison among key thermal sensitive points at random speed 1

However, the nut’s calculated temperature is generally higher than the experimental temperature. In contrast, the temperature calculation results for the fixed bearing tend to be lower than the corresponding experimental values most of the time. The discrepancies can be attributed to variations in parameters such as thermal conductivity, specific heat capacity, and heat transfer characteristics between the temperature model and the physical model in its operational state. The maximum relative errors between the calculated and experimental temperature for each working condition are presented in Table 4. Specifically, the maximum relative errors for

the nut, fixed bearing, and supporting bearing under different working conditions are 8.097%, 2.787%, and 1.275%, respectively. The results demonstrate that the temperature model applied to the thermally sensitive points of the ball screw exhibits acceptable accuracy, as indicated by the similarity between the fundamental trend of predicted data and the experimental data presented in the figure and further supported by the quantified error indicators within acceptable thresholds in the table. Consequently, this accuracy level facilitates the calculation and simulation of temperature rise during the actual operation of the ball screw and positions

**Table 4** Maximum relative error of calculated temperature on each work condition

	Random speed 1 (%)	Random speed 2 (%)	Step speed (%)	Constant speed (%)
Temperature of nut	8.097	7.282	7.553	7.336
Temperature of fixed bearing	2.600	2.452	2.172	2.787
Temperature of supporting bearing	0.774	0.791	1.275	0.938

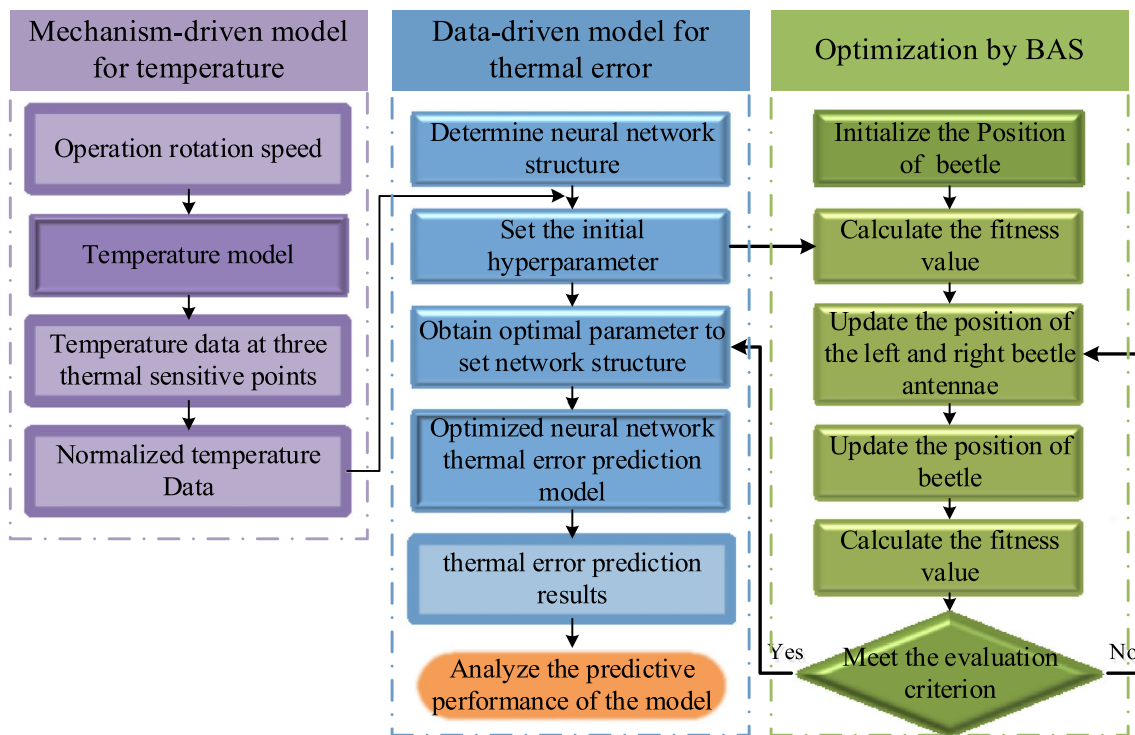


**Fig. 6** Flowchart of the hybrid-driven modeling process for thermal error prediction of ball screws

the proposed temperature model as a viable alternative to traditional temperature sensors. Furthermore, discrepancies between temperature calculated by the temperature model and real-world conditions can be improved and mitigated through subsequent application of data-driven modeling techniques designed to predict thermal errors.

## 2.3 Data-driven models for thermal error prediction of ball screws

### 2.3.1 Thermal error modeling

Various neural network models, including BP, LSTM, and convolutional neural network (CNN), are employed for predicting the thermal deformation of the ball screw due to their capability to perform regression prediction and handle time series data. In these data-driven models, the calculated temperature ( $T_{b1}$ ,  $T_{b2}$ , and  $T_N$ ) obtained from the temperature model under the random speed 1 and the experimental thermal deformation ( $D$ ) obtained from the thermal characteristic experiment under the random speed 1 are utilized as input and output data to construct the feature dataset required for model training. The calculated temperature and experimental thermal deformation data in full time series under the other three working conditions are employed as the test sets to evaluate the performance of the established data-driven

models. The developed data-driven models for full-time series thermal error prediction are employed to establish the mapping relationship between the calculated temperature of thermal sensitive points and thermal deformation. The dataset configurations, feature parameters, training, and testing methodologies of the models are kept constant to ensure a fair comparison among the three data-driven models. Additionally, the input and output data must be normalized before model training to mitigate the impact of data from different dimensions on the training outcomes. Lastly, the maximum number of training iterations is 100 to avoid excessive computational costs.

### 2.3.2 Hyperparameter optimization

Determining the optimal hyperparameters of the model is crucial for developing an accurate thermal error prediction model with optimal performance. Similar to other optimization algorithms, such as PSO and GA, the BAS algorithm can automatically search for the best solution. BAS algorithm is designed to mimic the movement of beetles towards the direction of antennae with strong odor signals, enabling efficient and rapid foraging. BAS can solve optimization problems quickly due to its simplicity and effective search process. Thus, in this study, the BAS algorithm is employed to optimize the hyperparameters of the thermal



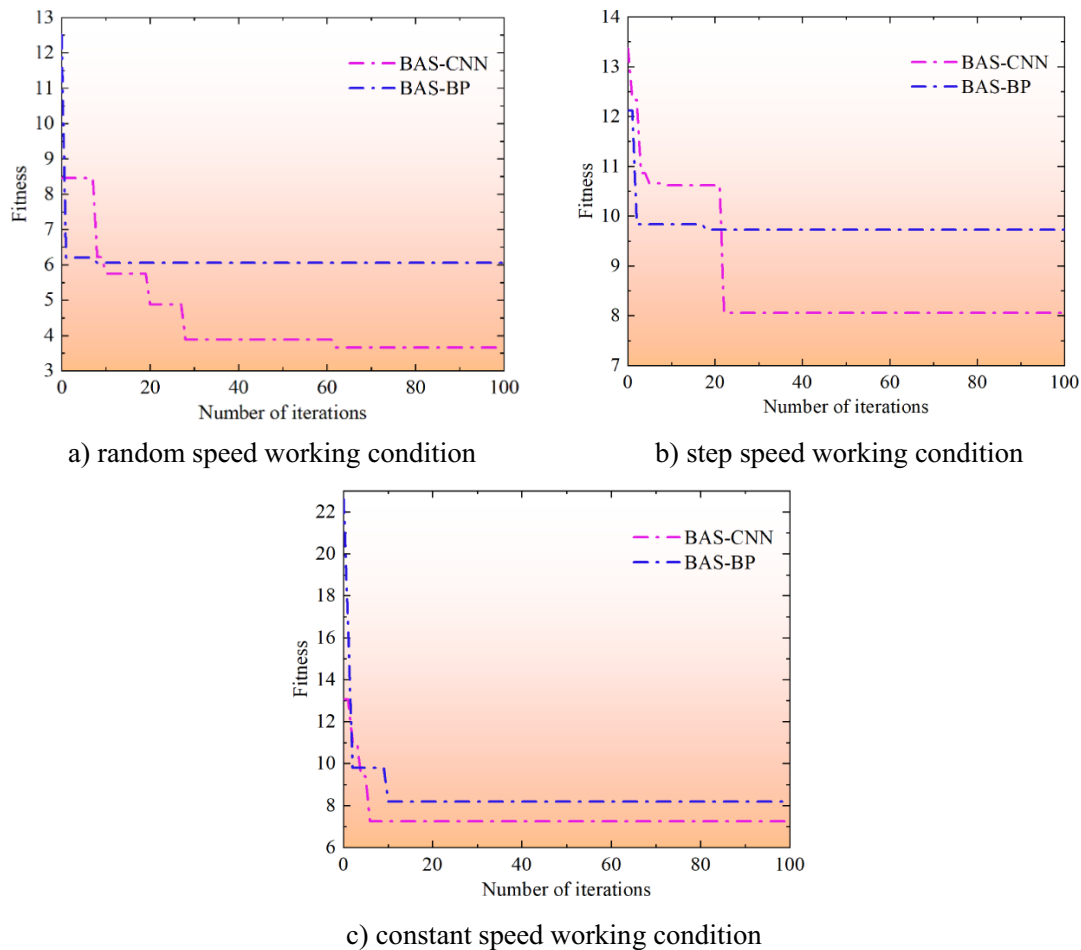


**Fig. 7** Adaptation curve of the optimization process under different working conditions

error prediction model for quick and automatic convergence towards high accuracy.

Since the prediction model based on the LSTM neural network exhibits abnormal and unacceptable prediction data during the initial prediction stage, the remaining two prediction models based on BP and CNN are further optimized by BAS. RMSE is utilized as the fitness function for hyperparameter optimization. The hyperparameters of the BP and CNN models are separately optimized to obtain the minimized RMSE value. In the CNN neural network, the optimized hyperparameters encompass the convolution kernel size for the two convolutional layers, the initial learning rate of the network, the learning rate decay factor, and the learning rate decay cycle. Simultaneously, the weights and thresholds of the BP neural network are optimized using the BAS algorithm to achieve the network's optimal prediction performance. Additionally, the maximum number of iterations for the BAS optimization algorithm is set to 100 to ensure efficient convergence and accuracy.

## 2.4 Thermal error prediction based on mechanism and data hybrid-driven model

Initially, the rotational speed data, serving as the working condition data, are input into the temperature model to generate time series temperature data for three thermal sensitive points. Subsequently, the obtained temperature data and thermal deformation in the axial direction measured by the eddy current displacement sensor are fed into various networks to train the data-driven models, including CNN, LSTM, BP, BAS-CNN, and BAS-BP. Then, the key hyperparameters of each network determined by the BAS optimization algorithm are input into the networks to obtain the optimal configuration of the models and predict a thermally induced error. The flowchart illustrating the process of hybrid-driven modeling for thermal error prediction of ball screws is presented in Fig. 6.

Figure 7 illustrates the changes in fitness of the two models in the model training stage during the optimization process

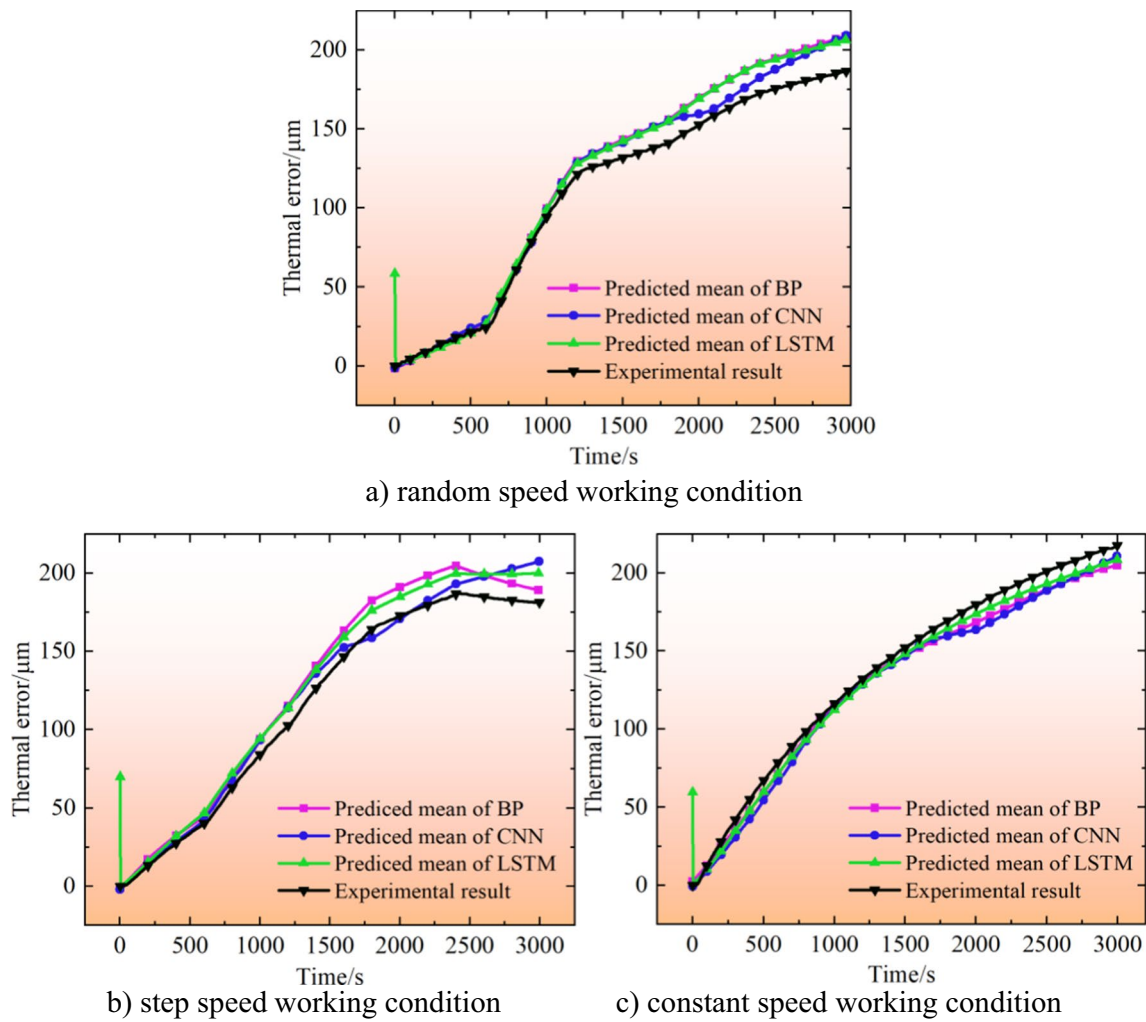


Fig. 8 Comparison between thermal error predicted mean results based on different neural networks

Table 5 RMSE results

Model	Random speed	Step speed	Constant speed
LSTM	12.4928	11.6939	6.2886
BP	13.1023	13.0666	8.2121
CNN	9.7497	9.0084	9.9612

Table 6 MAE results

Model	Random speed	Step speed	Constant speed
LSTM	10.3543	10.8388	5.8886
BP	10.7694	11.8556	7.1748
CNN	7.8414	7.1302	8.9819

across various operational conditions, providing compelling evidence of the algorithm’s effective convergence.

Three test data sets in full-time series corresponding to different working conditions are utilized to validate the accuracy of the established mechanism and data hybrid-driven model. The prediction results will be discussed in the next chapter.

### 3 Prediction results and discussion

Comparative analyses are conducted among hybrid-driven models based on different neural networks to assess the proposed mechanism and data hybrid-driven models’

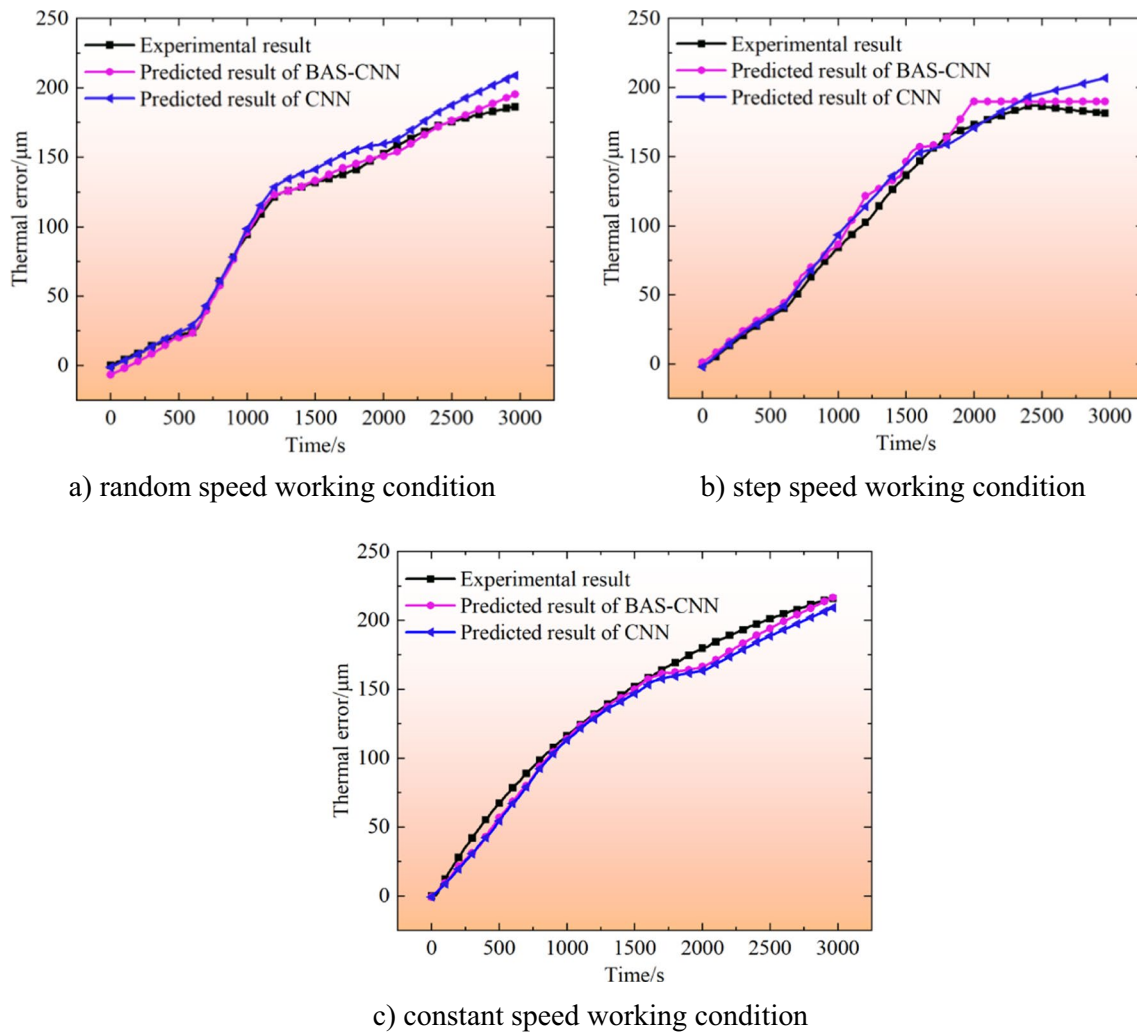


**Fig. 9** BAS-CNN-based thermal error prediction results for different working conditions

performance, validate the optimization algorithm's effectiveness, and determine the optimal model with the highest accuracy. The comparison results are then thoroughly examined and discussed.

### 3.1 Comparison between hybrid-driven models based on CNN, BP, and LSTM

The average thermal error values of the five predicted results from CNN, LSTM, and BP neural network prediction models under different working conditions are presented in Fig. 8 to compare the predicted results and performance of the mechanism and data hybrid-driven models. The prediction accuracy of all three hybrid-driven models is relatively high during the early prediction stage. In contrast, the prediction errors mainly occur in the latter half of the prediction process. Furthermore, the prediction results indicate superior performance of all three models under the constant speed

condition compared to other working conditions. Specifically, the CNN prediction model demonstrates the highest accuracy, followed by the LSTM and BP models. It is worth noting that the LSTM prediction model exhibits better overall prediction accuracy compared to others under the constant speed condition. However, it is characterized by occasional local deviation points in its prediction results.

Two evaluation metrics, RMSE and MAE, are employed to quantitatively assess the model's predictive performance. A lower value for these evaluation metrics indicates a higher accuracy of the established model. The evaluation results for the thermal error prediction model of the ball screw in the full-time series are presented in Tables 5 and 6. The model utilizing the CNN network as the data-driven framework demonstrates the closest alignment between the predicted and experimental results under random and step speed working conditions. This model exhibits superior performance

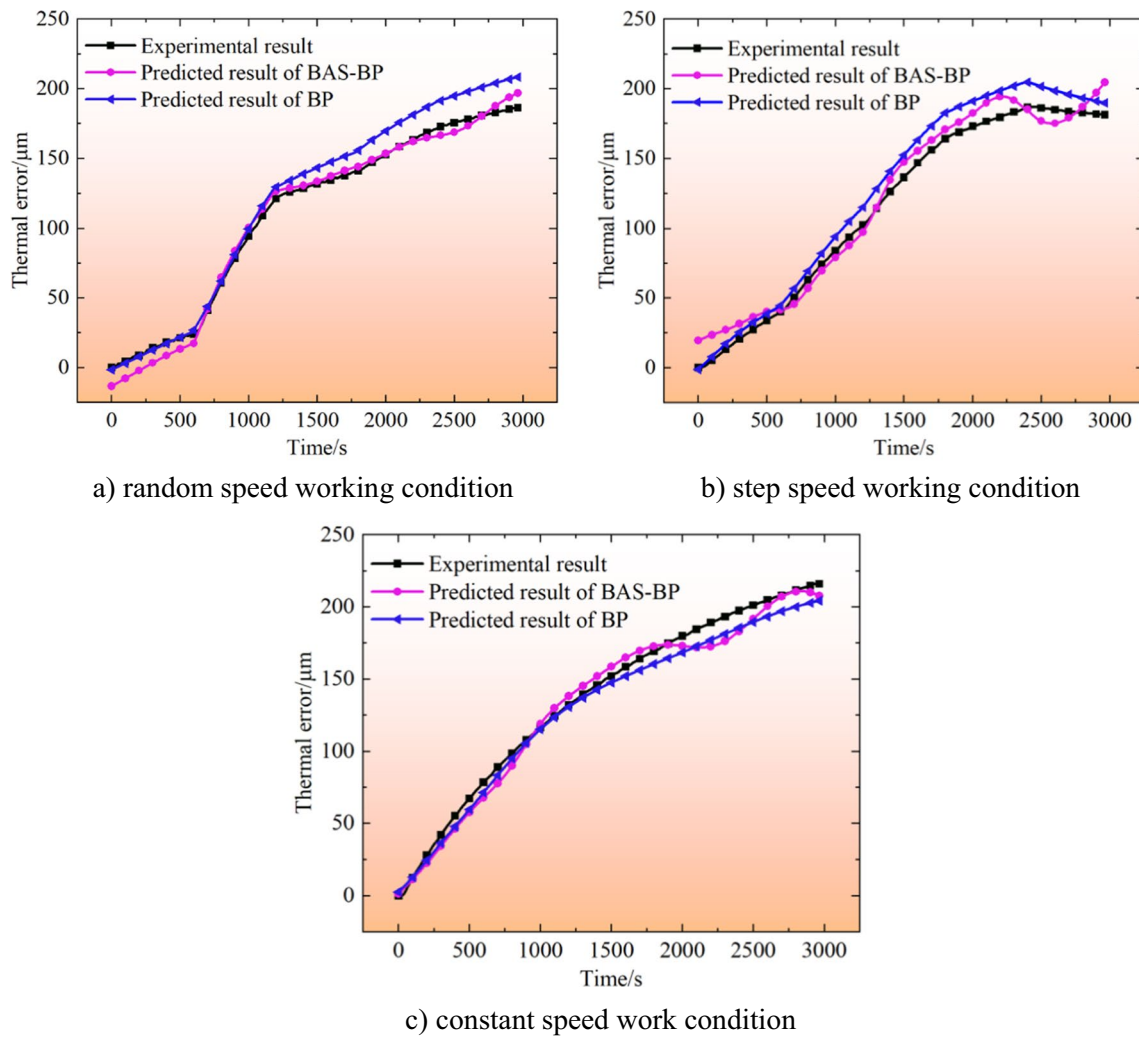


**Fig. 10** BAS-BP-based thermal error prediction results for different working conditions

compared to the other two hybrid-driven models. Moreover, the hybrid-driven prediction model based on the CNN neural network framework is characterized by a relatively stable prediction accuracy without any local mutation points observed during the initial prediction period (unlike the LSTM model).

In conclusion, the hybrid-driven prediction model with the CNN network as the data-driven framework exhibits the highest accuracy among the three models, particularly under random and step speed working conditions. This model demonstrates stable prediction accuracy in full-time series and avoids local mutation points observed in the initial prediction period of the LSTM model.

### 3.2 Comparison between optimized and unoptimized models

The predicted thermal errors of the ball screw under three working conditions obtained from the BAS-CNN, CNN, BAS-BP, and BP prediction models are compared with the corresponding experimental results. Figures 9 and 10 illustrate the comparison.

The thermal error prediction results based on the BAS-CNN and BAS-BP models demonstrate a closer alignment with the experimental values throughout the full-time series prediction than the unoptimized prediction model. The optimized models exhibit higher prediction accuracy and

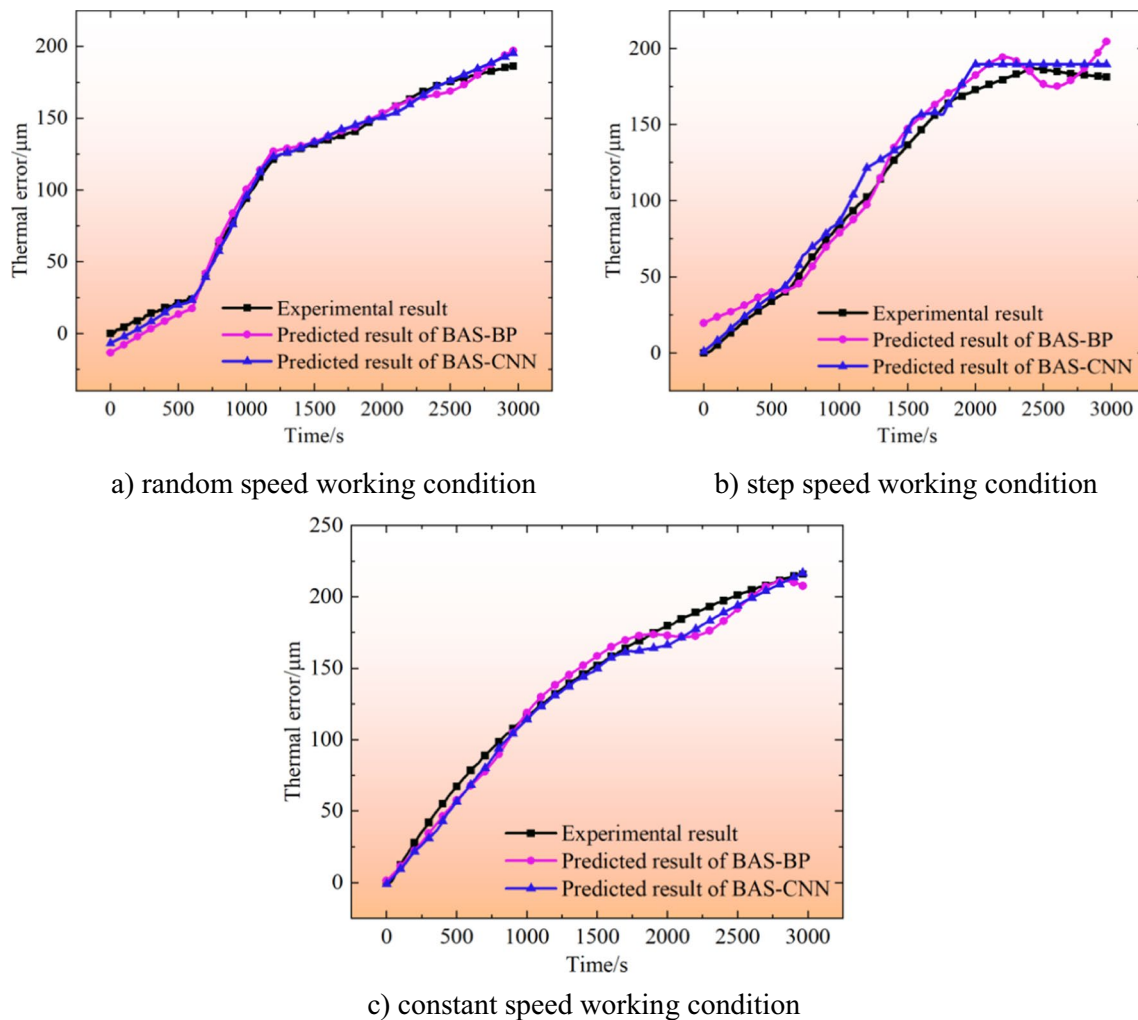


**Fig. 11** Comparison of thermal error prediction results based on BAS-CNN and BAS-BP

stability, validating the efficiency of the BAS-optimized algorithm. Although there may be some fluctuations in the predicted thermal error values compared to the experimental values under certain working conditions, these fluctuations have a limited impact on the overall prediction accuracy and stability.

### 3.3 Comparison between BAS-CNN and BAS-BP

The predicted thermal errors obtained from the BAS-CNN and the BAS-BP models under the same working conditions are compared with the corresponding experimental results in Fig. 11.

Both models exhibit favorable prediction performance under random and constant speed conditions. Both models

exhibit fluctuations in the predicted values for the step speed condition. However, the BAS-BP prediction model exhibits stages in certain prediction times that deviate from the observed trend of the experimental thermal error. Furthermore, the BAS-BP model displays higher prediction errors than the BAS-CNN model at the initial and final stages of the prediction process under random and step speed working conditions.

The distribution of relative and absolute errors in the prediction results of the BAS-CNN and BAS-BP models is presented in Figs. 12 and 13, respectively, to assess their full-time series prediction performance and reliability. It can be observed that the prediction errors under the three different working conditions are acceptable in engineering. Specifically, for the random, step, and constant speed



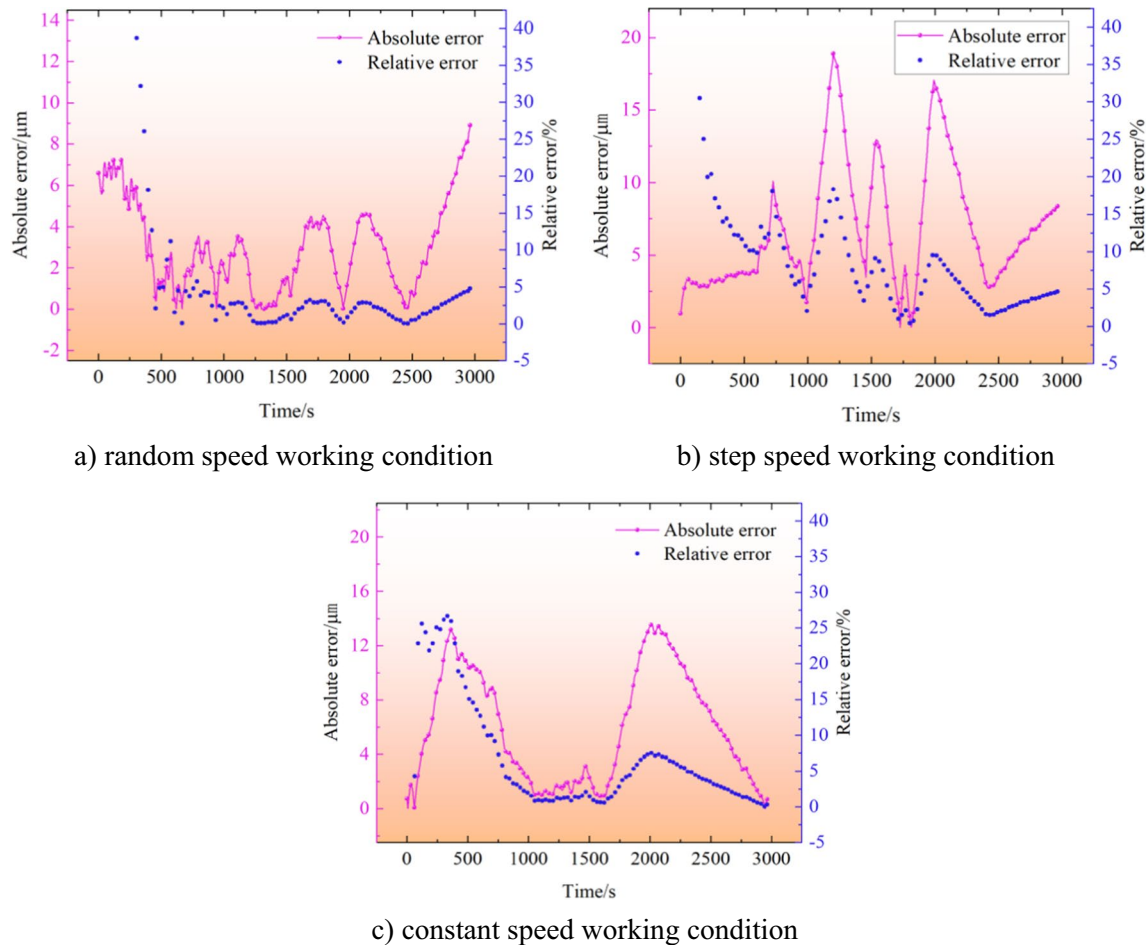


**Fig. 12** BAS-CNN-based error analysis of thermal error prediction for different working conditions

conditions, most absolute error values in the thermal error prediction results obtained from the BAS-CNN model are below  $5\ \mu\text{m}$ ,  $10\ \mu\text{m}$ , and  $9\ \mu\text{m}$ , respectively. Similarly, most absolute error values in the thermal error prediction results obtained from the BAS-BP model are below  $7\ \mu\text{m}$ ,  $12\ \mu\text{m}$ , and  $14\ \mu\text{m}$  for the respective working conditions. However, few absolute error values exceed the aforementioned thresholds. The maximum absolute errors in the prediction results of both models under the three working conditions are summarized in Table 7.

RMSE and MAE of both models were calculated to quantitatively compare the prediction performance of the prediction model before and after optimizing and to quantify the performance of the optimized model. The results are presented in Tables 8 and 9.

The optimized prediction model exhibits smaller RMSE and MAE values than the thermal error prediction model before hyperparameter optimization. Additionally, the RMSE and MAE values of the BAS-CNN model are consistently lower than those of the BAS-BP model under the three working conditions. It can be concluded that the

BAS-CNN model achieves high prediction accuracy and superior performance. Furthermore, the BAS-CNN model presented in this study consistently demonstrates relatively high predictive accuracy for thermal error prediction across various working conditions and random rotational speeds, emphasizing the model's excellent robustness.

## 4 Conclusions

Traditional thermal error neural network models face challenges in achieving full-time series prediction. Additionally, the existing thermal error modeling methods rely on operating temperature data at thermal sensitive points collected through a complex and costly temperature collection process. In this paper, a new mechanism and data hybrid-driven model using rotational speed as input data was proposed for the prediction of thermal-induced errors of ball screws in full-time series without temperature data

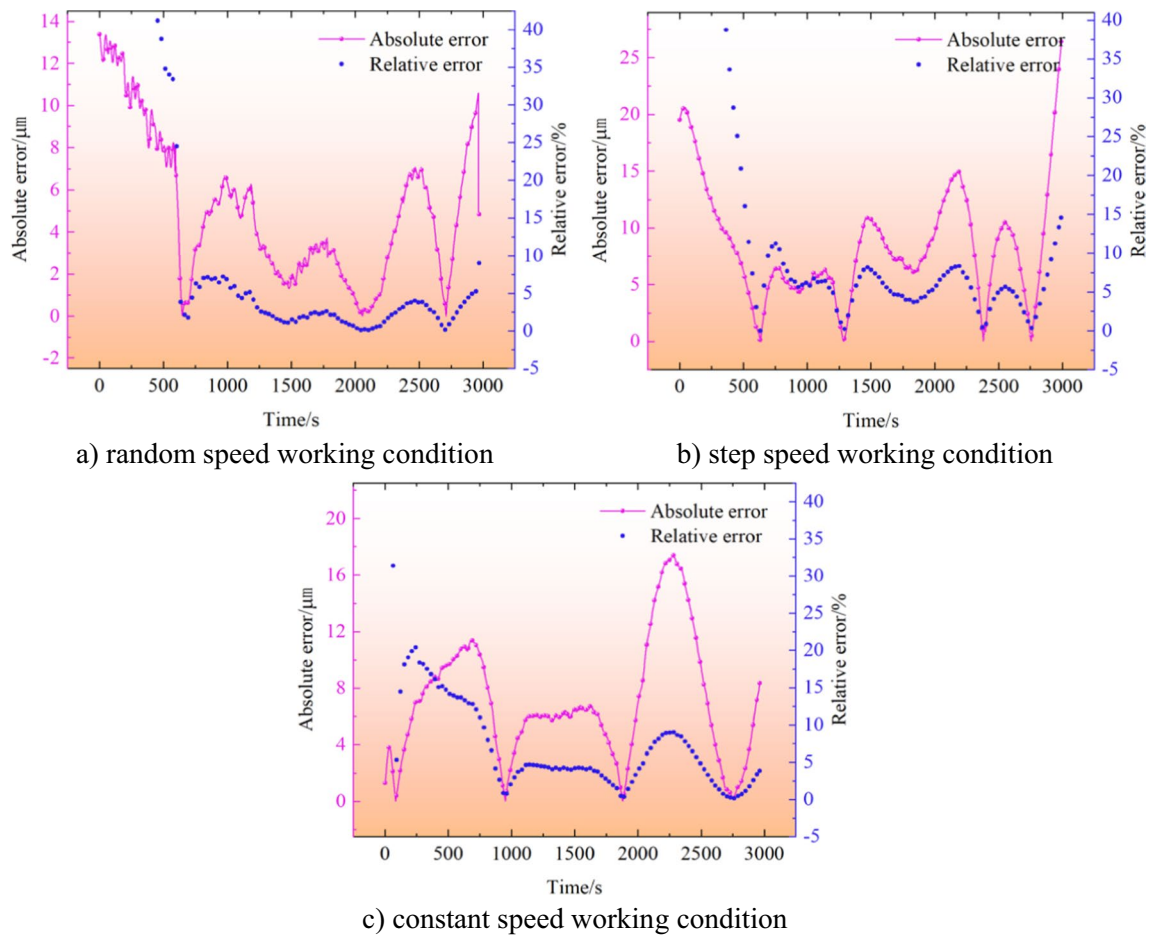


Fig. 13 BAS-BP-based error analysis of thermal error prediction for different working conditions

Table 7 Maximum absolute errors in the prediction results of two models

Model	Random speed (μm)	Step speed (μm)	Constant speed (μm)
BAS-CNN	9.01	18.90	13.51
BAS-BP	13.39	26.41	17.37

Table 8 RMSE results

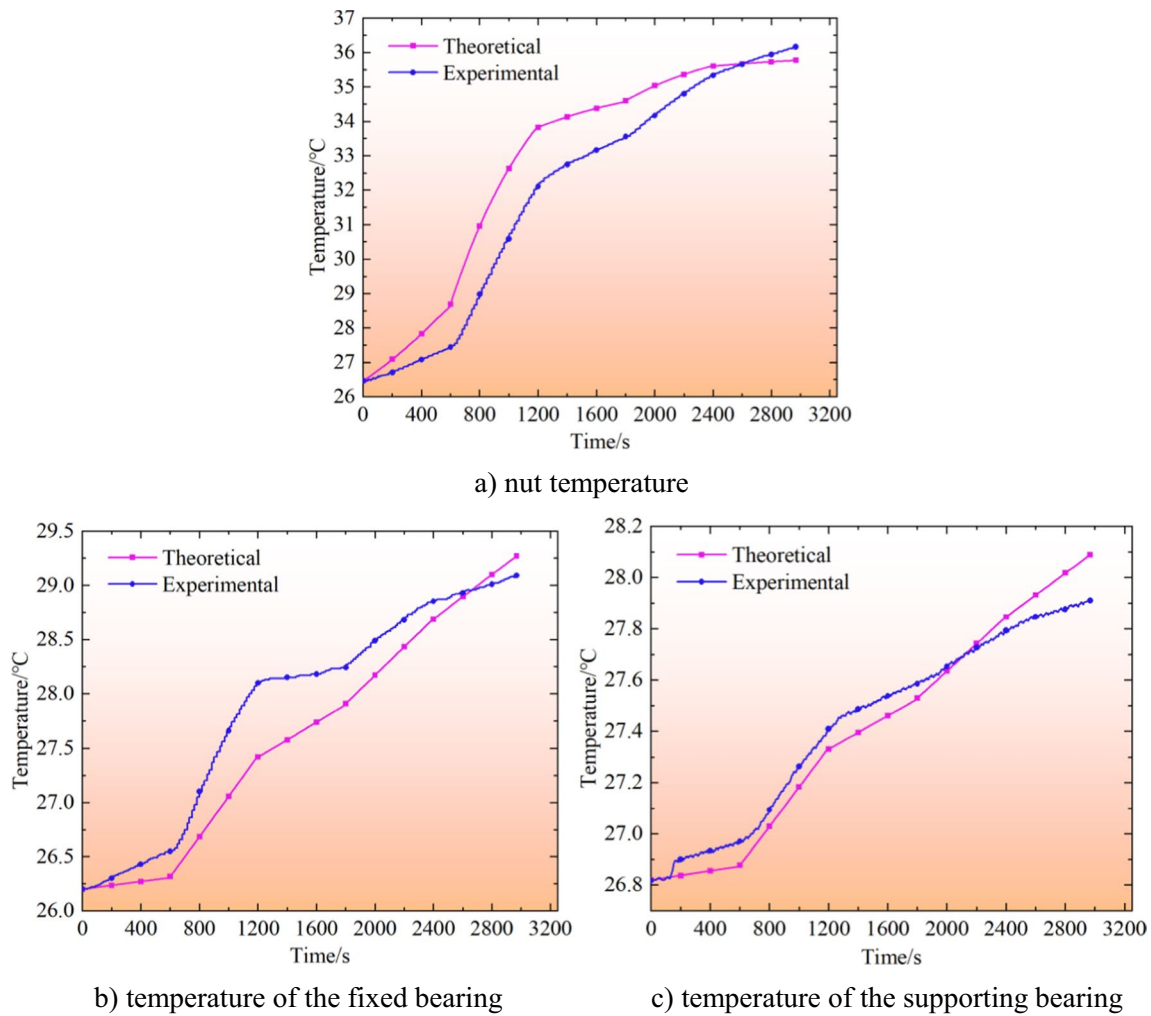
Data-driven model	Random speed	Step speed	Constant speed
BAS-BP	6.0480	9.7277	8.1902
BAS-CNN	3.6629	8.0580	7.2500

Table 9 MAE results

Data-driven model	Random speed	Step speed	Constant speed
BAS-BP	4.9750	8.4172	6.9879
BAS-CNN	2.9986	6.8731	5.9435

collection during operation. The following conclusions are drawn:

- (1) A mechanism and data hybrid-driven model for thermal error prediction of ball screws comprising the temperature model and the BAS-CNN was proposed. The model enables the prediction of thermal errors solely based on working condition data (specifically the rotational speed) without the requirement of collecting operating temperature data for ball screws.
- (2) A data-driven model based on BAS-CNN was proposed to achieve full-time series thermal error prediction of the ball screw. A comparison between the BAS-CNN model and the experimental data in full-time series demonstrates that the proposed model can accurately predict the thermal error of ball screws. Furthermore, the model exhibits excellent robustness, laying a solid foundation for thermal error compensation applications.
- (3) Comparative analyses were performed among the proposed hybrid-driven models based on different tra-



**Fig. 14** Temperature comparison among key thermal sensitive points at random speed 2

ditional neural networks. The results reveal that the hybrid-driven model utilizing BAS-CNN as the data-driven component achieves higher accuracy and lower error than CNN, BP, LSTM, and BAS-BP models. The BAS-CNN model exhibits the smallest RMSE and MAE values. Therefore, it can be concluded that the hybrid-driven model based on BAS-CNN outperforms the other models.

Even though this study provides a new thermal error prediction model architecture, the efficacy of thermal error compensation has not yet been assessed. Thermal error compensation will be explored in the subsequent research stages based on the proposed mechanism and hybrid-driven model, and its impact on reducing thermal errors will be evaluated.

## Appendix

The specific solution procedure of the temperature model for calculating the component's temperature increase at the location of the thermal sensitive point is as follows:

- (1) Calculating the bearing heat generation intensity  $Q_b$

The frictional heat generated by the bearing is one of the main heat sources in the ball screw. It is influenced by the frictional torque between the rolling elements, raceways, and retainers inside the bearing, as well as the stirring resistance of the lubricant. The heat generation of bearing can be expressed as follows:

$$Q_b = \frac{2\pi N M_b}{60} \quad (2)$$

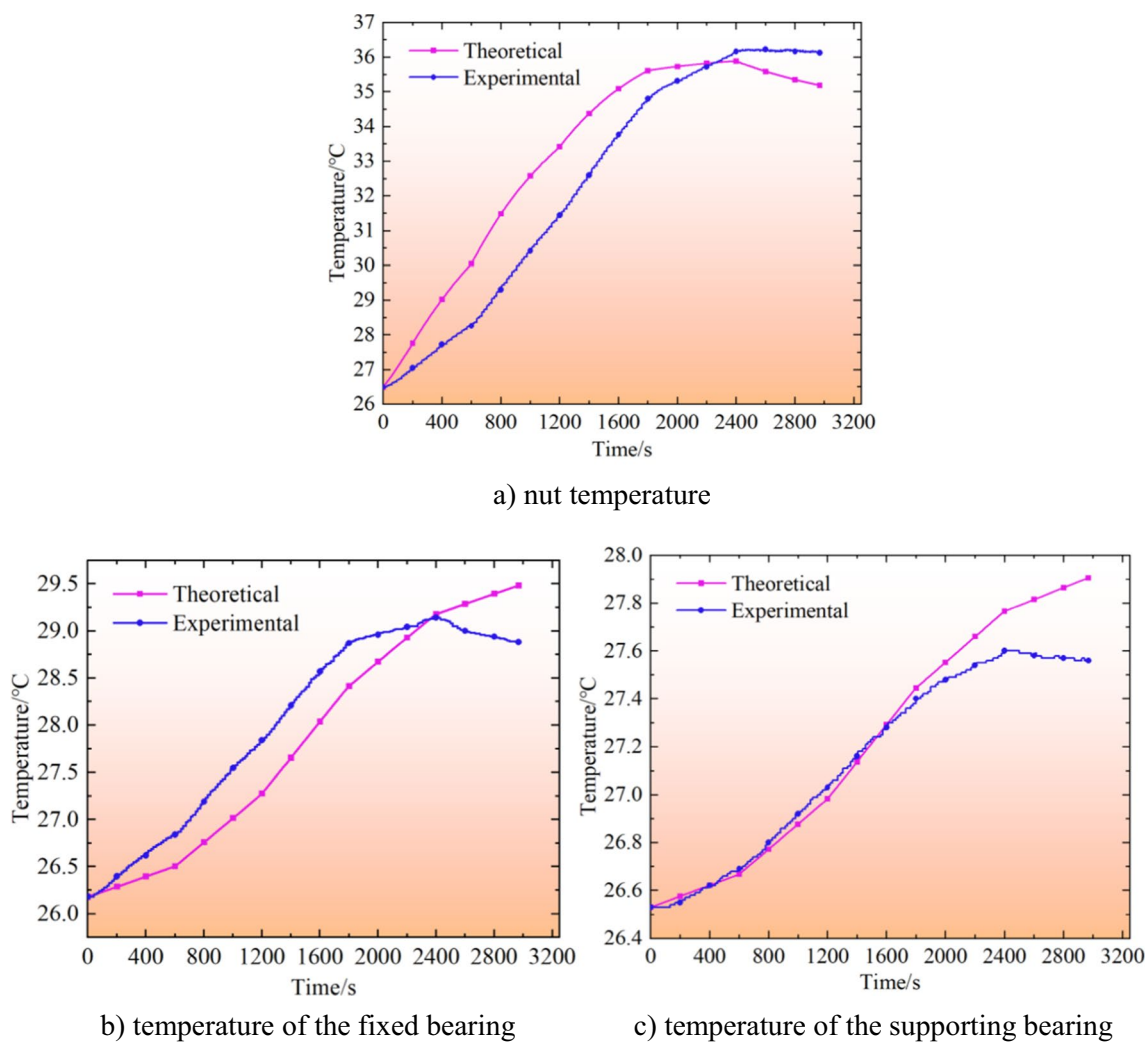


Fig. 15 Temperature comparison among key thermal sensitive points at step speed

where  $N$  represents the bearing’s rotational speed (r/min) and  $M_b$  represents the frictional torque of the bearing (N·m).

The frictional torque during the bearing’s operation primarily arises from rolling friction caused by material elastic hysteresis, friction induced by rolling element spinning and sliding, pure sliding friction in sliding contact areas, and viscous friction of the lubricant [26]. The frictional torque  $M_b$  mainly comprises  $M_0$  and  $M_1$ :

$$M_b = M_0 + M_1 \tag{3}$$

where  $M_0$  is the frictional torque related to the bearing type, rotational speed, and lubricant properties;  $M_1$  is the frictional torque associated with the bearing load.

Parameter  $M_0$  reflects the fluid dynamic loss of the lubricant and is calculated via Eq. (4).

$$\begin{cases} M_0 = 10^{-7} f_0 (\nu N)^{\frac{2}{3}} D_m^3 & \nu N \geq 2000 \\ M_0 = 160 \times 10^{-7} f_0 D_m^3 & \nu N < 2000 \end{cases}, \tag{4}$$

where  $D_m$  is the average diameter of the bearing (mm);  $f_0$  is a coefficient related to the bearing type and lubrication obtained from reference tables;  $\nu$  is the kinematic viscosity

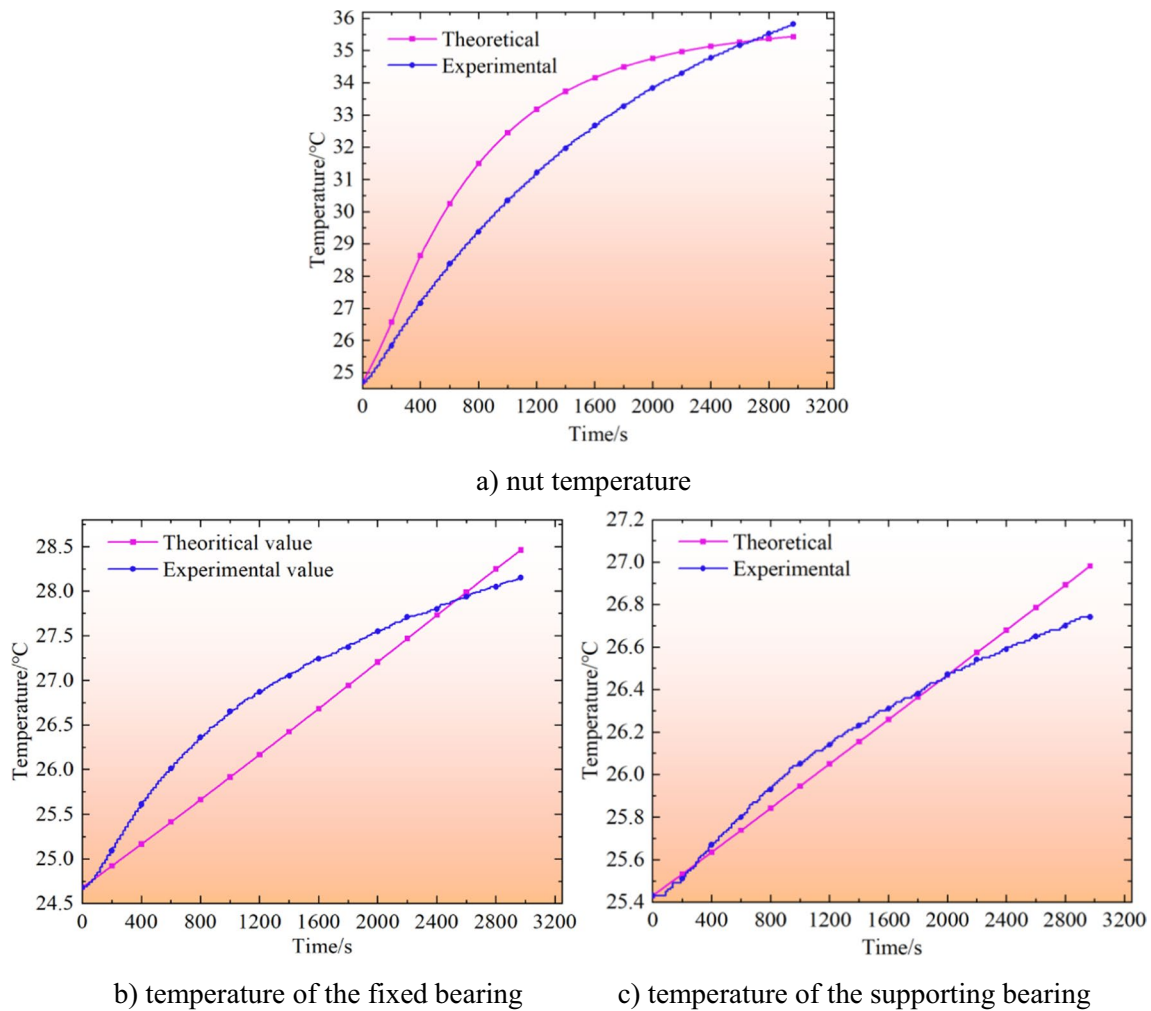


**Fig. 16** Temperature comparison among key thermal sensitive points at a constant speed

of the lubricant at the operating temperature of the bearing ( $\text{mm}^2/\text{s}$ ).

$M_1$  reflects frictional losses due to elastic hysteresis and differential sliding at the contact surfaces and can be calculated using Eq. (5).

$$M_1 = f_1 P_1 D_m \tag{5}$$

where  $f_1$  is a coefficient related to the bearing type and load, and  $P_1$  is the bearing load.

No axial load was applied in the experimental setup of the ball screw test bench used in this study. Therefore, the friction torque related to the load is neglected.

(2) Calculating the nut heat generation intensity  $Q_n$

The calculation of the nut heat generation intensity  $Q_n$  of the ball screw is closely related to its friction torque  $M$  and similar to calculating the bearing heat generation intensity:

$$Q_n = \frac{2\pi N M}{60} \tag{6}$$

where  $N$  represents the rotational speed of the ball screw ( $\text{r}/\text{min}$ );  $M$  represents the total friction torque of the ball screw ( $\text{N}\cdot\text{m}$ ) comprising the driving torque  $M_D$  and the resistance torque  $M_P$  exerted by the preloading force.

The driving torque  $M_D$  of the ball screw is the torque required to drive the nut to perform reciprocating motion by overcoming the axial load generated by the worktable mass and cutting forces:



$$M_D = \frac{F_D P_h}{2\pi\eta} \tag{7}$$

where  $P_h$  represents the lead of the ball screw (mm);  $F_D$  represents the axial force acting on the nut (N);  $\eta$  represents the transmission efficiency of the screw and the nut.

The resistance torque  $M_p$  of the ball screw is the torque required to drive the screw when the nut is preloaded, and there is no axial load:

$$M_p = \frac{F_p P_h}{2\pi\eta} (1 - \eta^2) \tag{8}$$

where  $F_p$  represents the axial preload force on the nut (N).

### (3) Calculating the heat generation in servo motors

Various losses in servo motors, including mechanical, electrical, and magnetic losses, are intrinsic factors contributing to heat generation. The heat generation in servo motors can be calculated using Eq. (9).

$$Q_M = \frac{M_T n}{9550} (1 - \eta) \tag{9}$$

where  $M_T$  represents the output torque of the servo motor (N·mm), and  $\eta$  represents the mechanical efficiency of the servo motor.

### (4) Convective heat transfer boundary conditions

Fixed components experience a temperature rise during system operation in the ball screw feed system. Some of these surfaces exchange heat with the surrounding air, a process known as convective heat transfer. Examples of such surfaces include bearing seats and motor enclosures. These components adhere to natural convective heat transfer principles in an unbounded space. The convective heat transfer can be expressed as follows [26]:

$$\begin{cases} Nu = C(Gr \cdot Pr)^n \\ Gr = \frac{g\alpha d^3 \Delta t}{\nu^2} \end{cases} \tag{10}$$

where  $Nu$  is the Nusselt number;  $Gr$  is the Grashof number;  $Pr$  is the Prandtl number;  $g$  is the acceleration due to gravity;  $\alpha$  is the volumetric expansion coefficient of air;  $d$  is the characteristic dimension;  $\Delta t$  is the temperature difference between the surface of the component and the surrounding air;  $\nu$  is the kinematic viscosity of air.

Parameters  $C$  and  $n$  in Eq. (10) can be selected based on the flow state of the fluid and the shape of the heat transfer surface.

During the nut’s operation, forced convection heat transfer occurs between its outer cylindrical surface and the surrounding air. The criterion correlation for the average convective heat transfer coefficient can be expressed as follows [27]:

$$\begin{cases} Nu = 0.906Re^{1/2} Pr^{1/3} \\ Re = \frac{ud}{\nu} \\ h = \frac{Nu \cdot \lambda}{d} \end{cases} \tag{11}$$

where  $Re$  represents the Reynolds number;  $u$  denotes the velocity of the air;  $h$  represents the convective heat transfer coefficient;  $\lambda$  represents the thermal conductivity of the air.

Figures 14, 15, and 16 illustrate the temperature comparison of key thermal sensitive points under other working conditions.

**Author contribution** Min Wang designed the study and wrote and reviewed this article. Wenlong Lu and Kuan Zhang conducted the experiments and established this model. Xiaofeng Zhu, Mengqi Wang, and Bo Yang established the experimental setup and reviewed this article. Xiangsheng Gao designed the study and supervised this work.

**Funding** The author(s) disclosed receipt of the following financial support for the research, authorship, and/or publication of this article: This study was supported by the National Natural Science Foundation of China (grant number: 51875008) and Guizhou Provincial Science and Technology Projects (grant number: ZK2024-ZD062).

**Data availability** Data are available from the authors upon reasonable request.

### Declarations

**Ethics approval** The article follows the guidelines of the Committee on Publication Ethics (COPE) and involves no studies on human or animal subjects.

**Competing interests** The authors declare competing interests.

### References

1. Ramesh R, Mannan MA, Poo AN (2000) Error compensation in machine tools—a review: part II: thermal errors. *Int J Mach Tools Manuf* 40(9):1257–1284
2. Weng L, Gao W, Zhang D, Huang T, Duan G, Liu T, ... & Shi K (2023) Analytical modelling of transient thermal characteristics of precision machine tools and real-time active thermal control method. *Int J Mach Tools Manuf* 186:104003
3. Pahk H, Lee SW (2002) Thermal error measurement and real time compensation system for the CNC machine tools incorporating the spindle thermal error and the feed axis thermal error. *Int J Adv Manuf Technol* 20:487–494
4. Liang Y, Su H, Lu L, Chen W, Sun Y, Zhang P (2015) Thermal optimization of an ultra-precision machine tool by the thermal

- displacement decomposition and counteraction method. *Int J Adv Manuf Technol* 76:635–645
5. Xu ZZ, Liu XJ, Kim HK, Shin JH, Lyu SK (2011) Thermal error forecast and performance evaluation for an air-cooling ball screw system. *Int J Mach Tools Manuf* 51(7–8):605–611
  6. Gallo A, Arana A, Oyanguren A, García G, Barbero A, Larrañaga J, Ulacia I (2013) Numerical modeling and design of thermoelectric cooling systems and its application to manufacturing machines. *J Electron Mater* 42:2287–2291
  7. Guo Y, Gao X, Wang M, Zan T (2021) Bio-inspired graphene-coated ball screws: novel approach to reduce the thermal deformation of ball screws. *Proc Inst Mech Eng, Part C: J Mech Eng Sci* 235(5):789–799
  8. Gao X, Qin Z, Guo Y, Wang M, Zan T (2019) Adaptive method to reduce thermal deformation of ball screws based on carbon fiber reinforced plastics. *Materials* 12(19):3113
  9. Min X, Jiang S (2011) A thermal model of a ball screw feed drive system for a machine tool. *Proc Inst Mech Eng C J Mech Eng Sci* 225(1):186–193
  10. Zhu J, Ni J, Shih AJ (2008) Robust machine tool thermal error modeling through thermal mode concept. *J Manuf Sci E-T ASME* 130(6):061006
  11. Huang T, Kang Y, Du S, Zhang Q, Luo Z, Tang Q, Yang K (2022) A survey of modeling and control in ball screw feed-drive system. *Int J Adv Manuf Technol* 121(5–6):2923–2946
  12. Li Y, Yu M, Bai Y, Hou Z, Wu W (2021) A review of thermal error modeling methods for machine tools. *Appl Sci* 11(11):5216
  13. Li Z, Yang J, Fan K et al (2015) Integrated geometric and thermal error modeling and compensation for vertical machining centers. *Int J Adv Manuf Technol* 76:1139–1150
  14. Pajor M, Zapłata J (2011) Compensation of thermal deformations of the feed screw in a CNC machine tool. *Adv Manuf Sci Technol* 35(4):9–17
  15. Jiang H, Yang JG (2010) Application of an optimized grey system model on 5-axis CNC machine tool thermal error modeling. In 2010 International Conference on E-Product E-Service and E-Entertainment (pp 1–5). <https://doi.org/10.1109/ICEEE.2010.5661570>
  16. Zhang EZ, Qi YL, Ji SJ, Chen YP (2017) Thermal error modeling and compensation for precision polishing platform based on support vector regression machine. *Modul Mach Tool Autom Manuf Tech* 58:48–51
  17. Ramesh R, Mannan MA, Poo AN, Keerthi SS (2003) Thermal error measurement and modelling in machine tools. Part II. Hybrid bayesian network—support vector machine model. *Int J Mach Tools Manuf* 43(4):405–419
  18. Mize CD, Ziegert JC (2000) Neural network thermal error compensation of a machining center. *Precis Eng* 24(4):338–346
  19. Hattori M, Noguchi H, Ito S, Suto T, Inoue H (1996) Estimation of thermal-deformation in machine tools using neural network technique. *J Mater Process Technol* 56(1–4):765–772
  20. Ma C, Zhao L, Mei X, Shi H, Yang J (2017) Thermal error compensation of high-speed spindle system based on a modified BP neural network. *Int J Adv Manuf Technol* 89:3071–3085
  21. Feng T, Ming Y, Ji P, Yabin W, Guofu Y (2018) CNC machine tool spindle thermal error modeling based on ensemble BP neural network. *Comput Integr Manuf Syst* 24(6):1383–1390 (In Chinese)
  22. Zhang HN (2019) Research on modeling of machining center spindle thermal error based on improved RBF network. *Tech Autom Appl* 38:60–74
  23. Zhang J, Li Y, Wang ST, Gou WD (2018) High-speed motorized spindle thermal error modeling based on genetic RBF neural network. *J Huazhong Univ Sci Technol (Natural Sci Edition)* 46(07):73–77
  24. Gao X, Guo Y, Hanson DA, Liu Z, Wang M, Zan T (2021) Thermal error prediction of ball screws based on PSO-LSTM. *Int J Adv Manuf Technol* 116(5–6):1721–1735
  25. Oyanguren A, Larranaga J, Ulacia I (2018) Thermo-mechanical modelling of ball screw preload force variation in different working conditions. *Int J Adv Manuf Technol* 97:723–739
  26. Lei Xiao (2016) The modeling and simulation research on comprehensive performance of hollow ball screw feed system, Huazhong University of Science and Technology). <https://kns.cnki.net/KCMS/detail/detail.aspx?dbname=CMFD201801&filename=1016919745.nh> (In Chinese)
  27. Holman JP (2008) *Heat Transfer (SI Units)*. Sie. Tata McGraw-Hill Education

**Publisher's Note** Springer Nature remains neutral with regard to jurisdictional claims in published maps and institutional affiliations.

Springer Nature or its licensor (e.g. a society or other partner) holds exclusive rights to this article under a publishing agreement with the author(s) or other rightsholder(s); author self-archiving of the accepted manuscript version of this article is solely governed by the terms of such publishing agreement and applicable law.